



Disturbance of Osteonal Remodeling in Atypical Femoral Fracture: A Short Review of Pathogenesis and a Case Report: Histomorphometric Analysis of Fracture Site

Hideaki E. Takahashi, Fumitaka Hirano,
Kayoko Furukawa Okuma, Yukichi Zenke,
Kunitaka Menuki, Hideo Ohnishi, Fumio Fukuda,
Akinori Sakai, Taketoshi Shimakura, Hiroshige Sano,
Yuta Tokunaga, and Noriaki Yamamoto

The present invited review was completed and submitted to the publisher on 13-Sep-20.

H. E. Takahashi (✉) · T. Shimakura · N. Yamamoto
Niigata Bone Science Institute, Niigata Rehabilitation Hospital, Niigata-shi, Niigata-ken, Japan
e-mail: hideaki.takahashi@aiko.or.jp;
taketoshi.shimakura@aiko.or.jp; nirehp.yamamoto@aiko.or.jp

F. Hirano
Department of Orthopaedic Surgery, Moji Medical Center, Kitakyushu-shi,
Fukuoka-ken, Japan

Department of Orthopaedic Surgery, University of Occupational and Environmental Health,
School of Medicine, Kitakyushu-shi, Fukuoka-ken, Japan
e-mail: hiroshinos@yahoo.co.jp

K. F. Okuma · Y. Zenke · K. Menuki · A. Sakai
Department of Orthopaedic Surgery, University of Occupational and Environmental Health,
School of Medicine, Kitakyushu-shi, Fukuoka-ken, Japan
e-mail: menuki@med.uoeh-u.ac.jp; a-sakai@med.uoeh-u.ac.jp

H. Ohnishi
Department of Orthopaedic Surgery, Moji Medical Center, Kitakyushu-shi,
Fukuoka-ken, Japan
e-mail: hareyan@mojih.johas.go.jp

F. Fukuda
Department of Orthopaedic Surgery, Kitakyushu General Hospital,
Kitakyushu-shi, Fukuoka-ken, Japan
e-mail: fukuda@seagreen.ocn.ne.jp

H. Sano
Niigata Bone Science Institute, Niigata Rehabilitation Hospital, Niigata-shi, Niigata-ken,
Japan

Department of Orthopaedic Surgery, Unuma Kikan Hospital, Minami Unuma-shi,
Niigata-ken, Japan

Y. Tokunaga
Niigata University of Health and Welfare, Graduate School, Kita-ku, Niigata-shi, Niigata-ken,
Japan

Keywords

Atypical femoral fracture · Bisphosphonates · Osteonal remodeling · Microcracks
Osteoclasts

1 Background

As the population of the elderly has been increasing in the world, treatment of osteoporosis has been quite important to prevent fragility fracture. An atypical femoral fracture (AFF) is one of the adverse effects of over suppression of bone turnover by the long-term use of bisphosphonates [1, 2] that frequently have been used for a long time because of their availability and price. The etiology of AFF still is not fully understood. Investigation of the fracture site can give a clue for understanding the mechanism of the AFF. As the authors had obtained a rare chance to study the site of the fracture, after a short review on radiological and histological findings, we report a case of an AFF with a histomorphometric assessment of the fracture site that shows a disturbance of osteonal remodeling.

2 A Short Review of Pathogenesis

Use of antiresorptive agents, bisphosphonates (BPs) and denosumab (Dmab), has contributed to the decrease of osteoporotic hip and spine fractures. However, AFFs located in the subtrochanteric and midshaft regions of the femur have been reported as one adverse effect in patients taking BPs [3] or Dmab [4]. A task force of the American Society for Bone and Mineral Research published reports in 2010 [5] and 2014 [6] on the epidemiology, pathogenesis, and medical managements of AFFs.

2.1 Radiological Findings

AFFs are not comminuted and present with a transverse fracture line at the point of origination on the lateral cortex. When the fracture spreads across the shaft to the medial cortex, and when it becomes complete, a prominent medial “spike” may be present. There may be a focal periosteal hypertrophy of the lateral cortex where the fracture initiated and recognized as cortical “beaking” adjacent to a transverse radiolucent fracture line [7].

Kwek EB et al. [8] described an insufficiency fracture consisting of (1) cortical thickening of the lateral side of the subtrochanteric region, (2) a transverse fracture, and (3) a medial cortical spike. In addition, nine patients (53%) had bilateral findings of stress reactions or fractures, and 13 patients (76%) had symptoms of prodromal pain. Lenart BA et al. [9] reported femoral bowing in 85.7% of AFFs. Associated findings of a periosteal beak and/or a black line, seen in 14.6%, were associated with increased fracture risk. Mohan et al. [10] described multifocal endosteal thickening of the femur in patients on long-term bisphosphonate therapy. Sato et al. [11] reported beaking in 15 femora of 10 patients (8.0%) with autoimmune diseases taking long-term glucocorticoids and bisphosphonates. Hagino et al. reported [12] radiographic beaking in 149 fractures (86.1%) in 230 patients treated with BPs and 17 fractures (37.8%) in patients who were not treated with BPs. Kumar G et al. [13] reported three cases of BP associated femoral stress fractures distal to an orthopedic implant. These patients presented with similar prodromal thigh pain and tension side cortical thickening. Although atypical fractures are known to occur in the femur following bisphosphonate therapy, Tan et al. [14] reported a case of atypical fractures in the tibia. Their case with juvenile idiopathic arthritis since childhood presented with bilateral atypical tibial fractures, followed by a later, single atypical fracture of the femur. This highlights a rare, but serious complication due to an antiresorptive agent. It also shows that teriparatide, while effective in increasing bone mass, does not fully prevent the development of atypical fractures.

2.2 Histological Findings

There have not been many reports on the histology of AFFs, particularly the fracture line itself. Somford et al. [15] showed a marked increase in resorption at the cortex biopsied about 1 cm from the fracture site, which was considered a cause of weakness of the bone. Aspenberg P et al. [16] reported a case with frozen bone with remodeling at the crack. They described sections parallel to the cortical surface analyzed every 5 mm from the periosteum to the endosteum. The intact bone 7 mm distant from the fracture showed a regular osteonal structure with most of the lacunae empty. There were numerous irregular small cracks in the osteocyte-less matrix. The fracture appeared mostly as a meandering empty crack, only 0.1 mm wide or less. The bone in its vicinity in the cortex contained numerous resorption cavities with loose marrow. Many of these contained large osteoclasts, sometimes with extremely large numbers of nuclei and with detachment from the underlying bone

surface. Jamal et al. [17] reported the presence of double label after tetracycline labeling in a biopsied specimen at a site just below the point of fracture. Kajino et al. [18] investigated a biopsy from a complete fracture including the fracture surface. They found immature bone on the periosteal surface and reported that almost no TRAP-positive cells could be found.

Schilcher J et al. [19] described histology of eight cases of AFF. All incomplete fractures showed a fracture gap with a width of 180 (150–200) μm . Fragments of lamellar or woven bone in the gap and newly formed woven bone adjacent to the fracture line were found. Osteoclasts were frequently found close to the fracture line and less frequently further away. Resorption cavities in the cortex were common (Fig. 1). Adjacent to the fracture, they were smaller and tended to be oriented parallel to the fracture plane, while farther away from the fracture they were larger and tended to be oriented perpendicular to the fracture line (Fig. 2). All samples showed a callus reaction on both the endosteal and the periosteal aspects of the fracture. The callus consisted mainly of woven bone and soft tissue. The periosteal bony callus was interrupted where the fracture reached the periosteal surface. The crack was thin and mainly contained amorphous acellular material, and some traces of bony fragments. The surrounding bone showed signs of remodeling, mainly represented by the presence of osteoclasts, resorption cavities, and woven bone facing the crack. It was striking that there were no signs of remodeling or callus formation within the fracture gap itself, despite the cellular activity in the adjacent tissue. Their microCT image of the biopsied core (Fig. 1), 11.4 mm in diameter [20], shows numerous pores in the upper half of the specimen and probably in the lower half, too. Kondo N et al. [21] reported histomorphometric assessment of nine BP-treated cases of AFFs, five subtrochanteric and four diaphyseal cases, in patients treated with glucocorticoids (GC). Bone formation was decreased more severely in the former than in the latter due to the higher GC doses used.

Using the CT-based finite element method, Oh Y et al. [22] demonstrated that significant tensile stress caused by bowing of the femoral shaft is associated with AFFs. Oh Y et al. [23] reported the location of AFF injury could be determined by individual stress distribution influenced by femoral bowing and neck-shaft angle.

Fig. 1 3D reconstruction of a bone biopsy with microCT. The fracture line (gap) in the middle of the biopsy core runs horizontally and is surrounded by a periosteal callus reaction (yellow square). Numerous enlarged resorption pores (blue triangles) can be seen from the fracture line to the tip of the core. (Reproduced with permission from Dr. Schilcher)

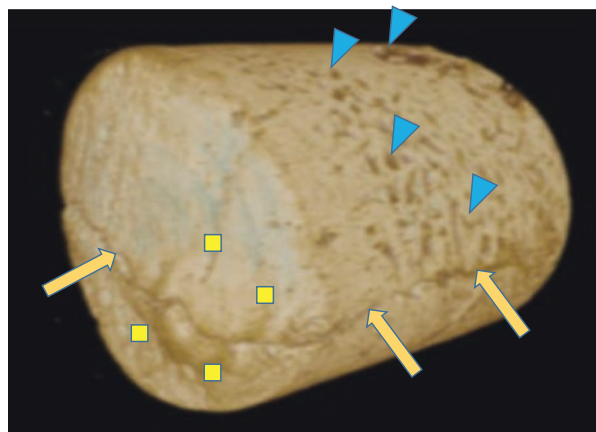
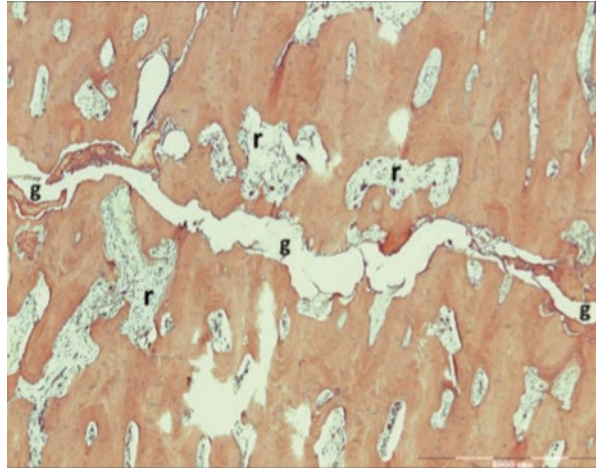


Fig. 2 Numerous and enlarged pores.

Resorption cavities (r), forming osteons and Haversian canals on both sides of the fracture gap (g). (Reproduced with permission from Dr. Schilcher)



Oh Y. et al. [24] proposed a classification of atypical femoral fracture subtypes. Although all cases in this study, both a midshaft group ($n = 18$) and a subtrochanteric group ($n = 19$), met the criteria of AFF by ASBMR criteria, five cases of the midshaft group had no history of exposure to bisphosphonates, but did have significantly greater femoral bowing. Histology of the fracture sites was reported in 12 cases, describing enchondral ossification and bone remodeling. A longitudinal section of the biopsied specimen in figures in the report shows many enlarged cavities mostly extended longitudinally from fracture line about 6 ~ 7 mm each side, total of 12.5 mm, the full extent of the figure (Fig. 2a, c [24]). Some cavities contain osteoclasts, osteoblasts, and fragments of cartilage. Thus, biomechanical environment focally gives extensive effects to make resorptive cavities and tunnels.

3 A Report of a Case

Histomorphometric assessment of a fracture site of an AFF case.

3.1 Introduction

We analyzed bone specimens obtained from the fracture site of this case, using bone histomorphometry.

3.2 Materials and Methods

3.2.1 Patient Background and Surgery

The patient was an 83-year-old Japanese woman with osteoporosis, treated with Risedronate and Alfacalcidol for the previous 5 years. She started to have left lateral thigh pain and claudication following a low-energy fall 4 months prior to admission. Radiographs revealed thickening of the lateral cortex and a transverse radiolucent

fracture line in the diaphysis (Fig. 3-1, 4). In 2007 she had bilateral knee arthroplasty. In addition, the contralateral thigh showed significant femoral bowing. The fracture fulfilled the ASBMR task force revised criteria for atypical femoral fractures [6]. By MRI, there was a high intensity signal 1 cm long on the lateral cortex on a T2WI image (Fig. 3-2,3). The patient had normal levels of bone resorption and formation markers except for low 25(OH) Vitamin D. She suffered from CKD, and a DXA showed low BMD of the hip and lumbar spine (Table 1).

After admission, Risedronate was discontinued and Tetracycline hydrochloride was orally administered on a 02-08-02-08 schedule. As anterograde intramedullary nailing was difficult because of excessive femoral bowing, a corrective osteotomy and intramedullary nailing were performed. During surgery, the site of the transverse radiolucent fracture line was soft and fragile, and transparent effusion was observed by finger-pressure to the protruded cortex. After reaming, a biplanar closed wedge osteotomy (longitudinal width: 5 mm/angle: 10 degrees) and osteosynthesis was performed using an anterograde femoral nail. To bridge the gap of the

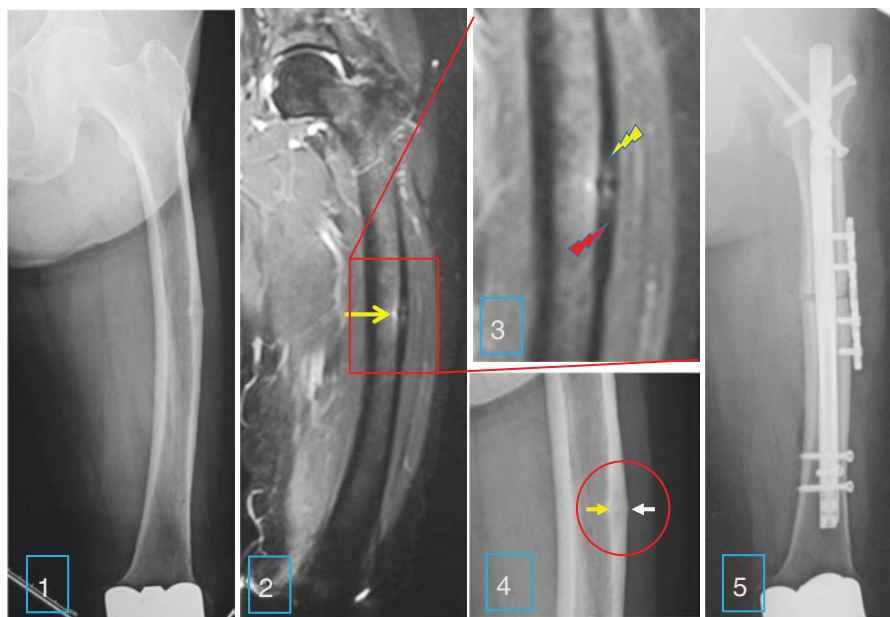


Fig. 3 Preoperative X-ray, MRI, and postoperative X-ray. **1** Preoperative X-ray of the left femur, with lateral bowing and hypertrophy of the lateral cortex on both periosteal and endocortical surfaces of the midshaft. **2** Preoperative MRI of the left femur, showing high intensity area in the bone marrow adjacent to the mid-lateral cortex (yellow arrow). **3** Preoperative MRI of the left femur, showing high intensity area in the intracortical region of the mid-lateral cortex (upper end: yellow arrow; lower end: red arrow). **4** Preoperative X-ray of the left femur. An enlarged image of the midshaft, indicating the hypertrophy of both periosteal (white arrow) and endocortical (yellow arrow) surfaces. **5** Postoperative X-ray of the left femur: lateral bowing was corrected and fixed with intramedullary rodding and plate fixation

Table 1 Laboratory data on admission

Biochemical markers at the time of admission		
Parameters	Results	Reference range
Serum calcium (mg/dL)	10.2	8.7–10.3
Serum phosphorous (mg/dL)	3.5	2.5–4.7
Serum alkaline phosphatase (U/L)	219	115.369
Serum TRACP-5b (mU/dL)	335	120.420
Serum P1NP (Ig/L)	17.9	17.0–64.7
Serum ucOC (ng/mL)	2.48	<4.50
Serum homocysteine (nmol/mL)	10.8	5.1–11.7
Serum pentosidine (pg/mL)	0.15	9.2–43.1
25(OH)Vit.D (ng/ml)	17.0	30–100

P1NP = procollagen type 1 N-terminal propeptide

TRACP-5b = tartrate-resistant acid phosphatase type 5b

ucOC = uncarboxylated osteocalcin

BMD: L2–4:0851 g/cm² (%YAM; 84%); left femur, neck 0.419 g/cm² (%YAM; 53%)

Total 0.696 g/cm² (%YAM; 81%)

osteotomy site and to acquire rotational stability, decortication and local site plating fixation were added (Fig. 3-5). The bone fragment excised at osteotomy broke into 2 pieces on removal and was preserved for bone histomorphometry.

3.2.2 Bone Histomorphometry

Assessments of Cortical Bone

Assessments of Endocortical Lamellar Bone

The lateral osteotomy piece was fixed in 70% ethanol, stained with Villanueva bone stain and embedded in methylmethacrylate without decalcification [25, 26]. The embedded lateral piece was sectioned at a thickness of 300 µm in the horizontal direction perpendicular to the shaft using Maruto's Micro Cutter MC 201. The thickness of the blade was 600 µm. The bone sample was ground to a thickness of 30 µm (Section L I). After the section L I was made, a radiograph of the rest of the block showed a linear radiolucent zone at the edge of the block, revealing an incomplete fracture line of the lateral cortex. Two more sections were made (Sections L II and L III) based on the finding of the fracture line in this region. A photograph of all three sections was made using bright light, fluorescent and polarized microscopy for comparison.

Observation of the Three Sections Three ground sections were available for observation. Each section had different characteristics because of its location with respect to the radiolucent line (the incomplete fracture line) in the lateral cortex. The L I section was located about 1 mm from the L II section, which included the edge of the radiolucent line. The L III section included the other side of the radiolucent line. The radiolucent line was about 1 mm in thickness, located between L II and L III.

Criteria

In this case, many enlarged intracortical pores in the lateral cortex demonstrated abnormal remodeling. Subsequently, novel criteria [27] were developed to assess the size of each pore, how much cumulative bone resorption had occurred, and whether bone formation was occurring at the time of fracture. We could also determine whether bone formation had occurred before the labeling period but had stopped at the surgery or had not occurred at all after the reversal-resorptive period. A quiescent surface is usually covered with lining cells (inactive osteoblasts) during the normal remodeling cycle, so we used the term “inert” in this report to indicate pore surfaces where neither osteoclasts nor osteoblasts were observed.

A type 1d pore is defined as a pore with double label (dLS) in lamellae parallel to the inner surface (Figs. 4 and 5), with either circumferential formation on the

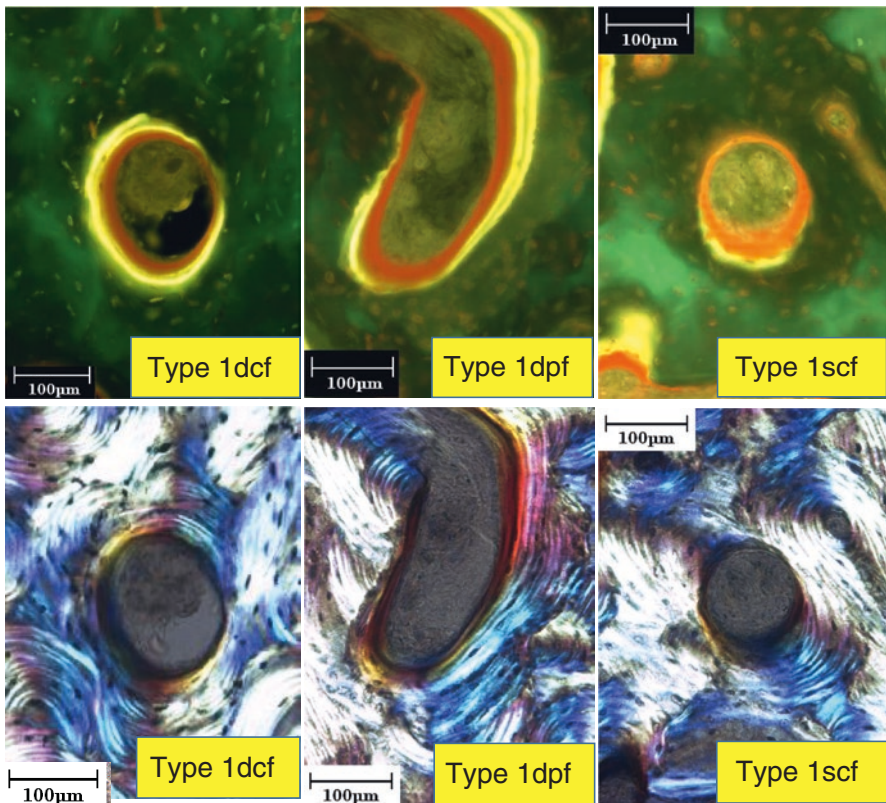


Fig. 4 Type 1d, 1s, and 1o pores. Type 1d pore is defined as a pore with double label in lamellae parallel to the inner surface, either circumferentially formed on the entire surface (type 1dcf) or partially formed with other phases of the remodeling cycle, which could be single label, osteoid, erosion, or an inert surface (type 1dpf). A type 1s pore is defined as a pore with single label in lamellae parallel to the inner surface, either circumferentially on the entire surface (type 1scf) or partially with other phases of a remodeling cycle (type 1spf), but not double label. Both type 1d and 1s are observed under fluorescent light

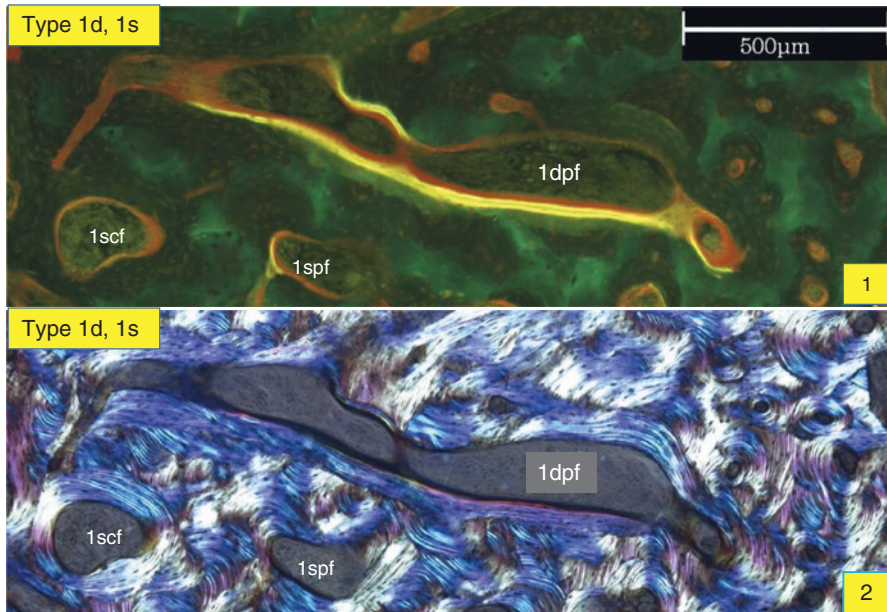


Fig. 5 Transversely extended type 1 pore in a transverse section. The main feature of the 1d pore is a double labeled surface, but can also have a single label and osteoid surface. This type 1d pore, even though large, shows the capability of lamellar bone formation on a partial surface, and may be called the type 1d with partial formation (type 1dpf) on the inner surface. (1, fluorescent light; 2, polarized light)

entire surface (type 1dcf) or partial formation (type 1dpf). In cases of partial formation, the remainder of the surface might be in other phases of the remodeling cycle, which could be single label (sLS), osteoid surface (OS), eroded surface (ES), or inert surface (IS). A type 1s pore is defined as a pore with single label (sLS) in lamellae parallel to the inner surface, with either circumferential formation on the entire surface (type 1scf) or partial formation (type 1spf) with other phases of the remodeling cycle. The type 1o has an osteoid seam, observed under bright light field, but was not counted separately because of the thickness of the sections.

A type 2 pore is defined as a pore with lamellae parallel to the inner surface, with either circumferential formation on the entire surface (type 2cf) or partial formation (type 2pf), but with non-parallel lamellae on the rest of the surface (Fig. 6). A type 3 pore has non-parallel lamellae on its entire inner surface. A type 4 pore is a cavity with an irregular and disrupted surface composed of fragmented osteonal structure. This may be the result of the coalescence of many large pores containing fragments of lamellar bone and debris inside (Figs. 6-4, 5, 8-5, and 13-1). Each pore was assessed by type and its size measured. The classification of pore types for measurement was limited to only 1d, 1s, 2, 3, and 4 for simplicity (Table 2).

Figures 7 shows a secondary osteon in longitudinal section of rib cortex of a dog stained by tetrachrome stain under bright light (Fig. 7-1) and a fluorescent light

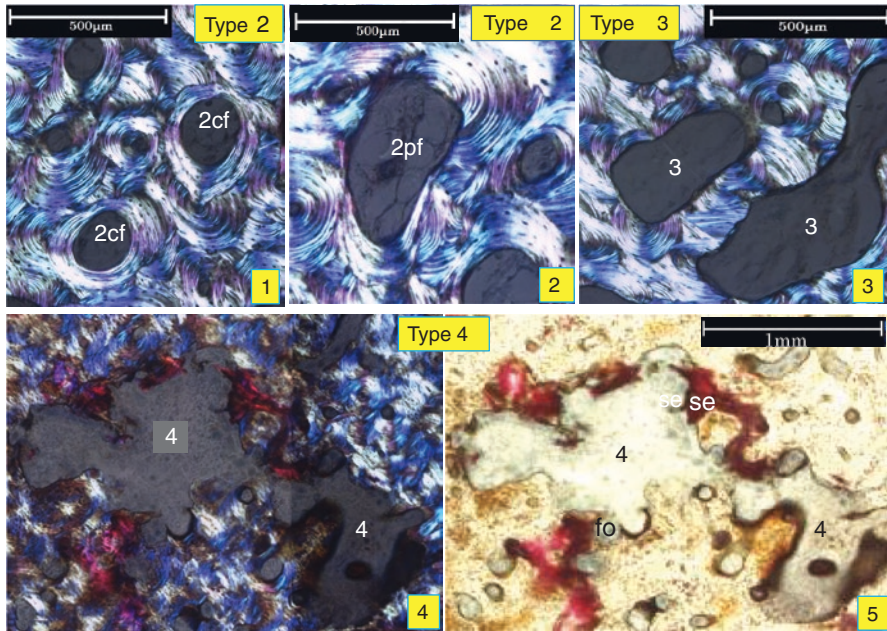


Fig. 6 Types 2, 3, and 4 under polarized light microscopy. The type 2 pore shows lamellae parallel to the inner surface, either circumferentially formed on the entire surface (type 2cf) (1) or partially formed (type 2pf) (2) with other phases of a remodeling cycle, which could be osteoid, erosion, or an inert surface. Nevertheless, parallel lamellae are observed and bone formation has finished before labeling. The type 3 pore shows lamellae that are parallel to the inner surface, circumferentially on the entire surface (3). The type 4 pore shows an irregular inner surface, which could be an eroded Haversian canal surface, fragmented osteons (fo), and bone debris with stained effusion (se) (4, polarized light; 5, bright light)

(Fig. 7-2) with double label. R shows a part of the resorption phase, RR indicates the reversal/resorptive phase in the cutting cone and F shows a part of the formative phase in the closing cone. Figure 7-3, 4 shows the osteon in the transverse section.

Figure 8-1, 3 illustrates in longitudinal section a cutting cone with primary osteoclasts at the tip targeting a microcrack and secondary osteoclasts at the side wall. A pore with double label (type 1d), single label (type 1s), and osteoid seam (1o), respectively, and with lamellae parallel to the inner surface of the pore (type 2) or without parallel lamellae (type 3) can also be seen. Figure 8-2, 4 illustrates, in the transverse section of a closing cone, the same relation between types 1, 2, and 3 in the transverse plane of the closing cone.

Assessments

Under bright field at $\times 20$ magnification, the size of each pore was measured histomorphometrically using “TP Measure” (System Supply, Nagano, Japan) and an epifluorescent microscope (Olympus BX50, Olympus Corporation, Tokyo, Japan) with a polarized attachment. Simultaneously, each pore type was classified under polarized light, at both $\times 20$ and $\times 100$ magnification. A map of each section under polarized light was made combining 150 ~ 250 visual fields under $\times 100$ magnification.

Table 2 Classification of types of intracortical pores

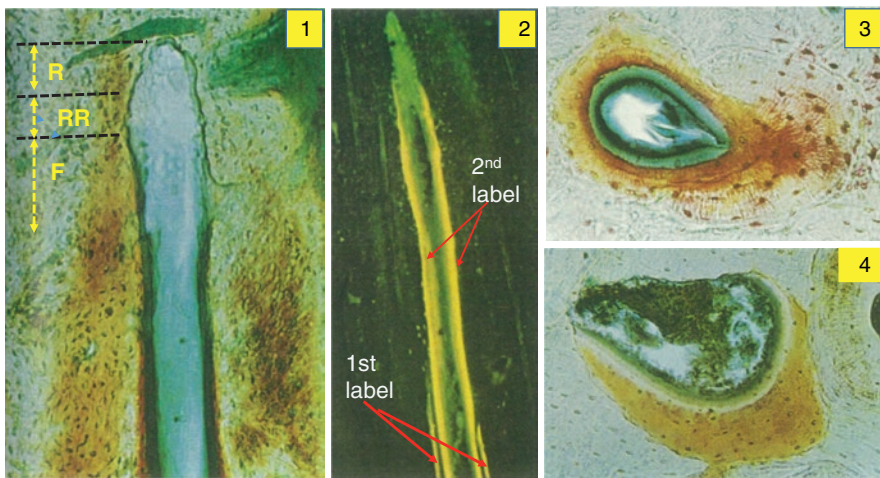
Labels ^{a/} Osteoids ^b		Lamellar bone formation ^c		Characteristics of inner surface	
Type		Subtype	On inner surface of a pore	Direction of lamellae	Other surfaces
1d	Double	1dcf	Circumferential formation	Parallel	
		1dpf	Partial formation	Partially parallel	sLS, ES, OS
1s	Single	1scf	Circumferential formation	Parallel	
		1spf	Partial formation	Partially parallel	ES, OS
1o	Osteoid	1ocf	Circumferential osteoid formation	Parallel	
		1opf	Partial osteoid formation	Partially parallel	ES, IS
2	Non	2cf	Circumferential formation	Parallel	
		2pf	Partial formation	Partially parallel	ES, IS
3	Non	–	No formation	Non parallel	
4	Non	–	No formation	Irregular	

^aFluorescent light

Observed ^bBright light

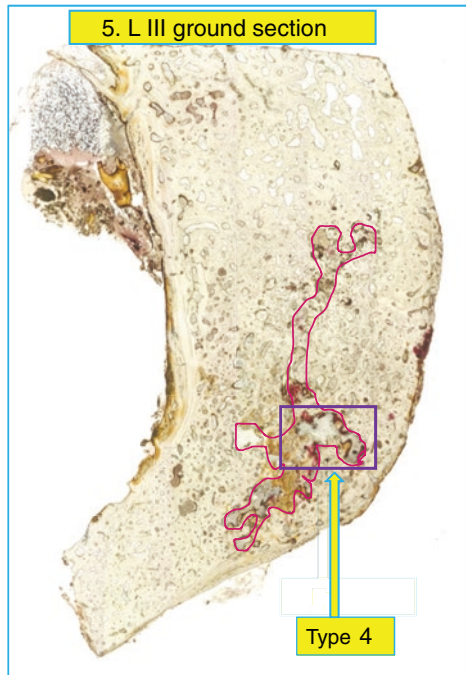
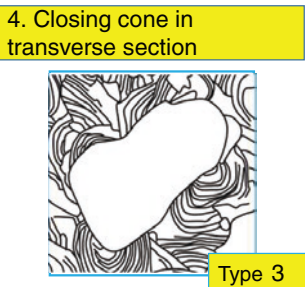
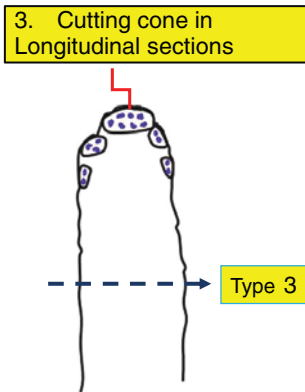
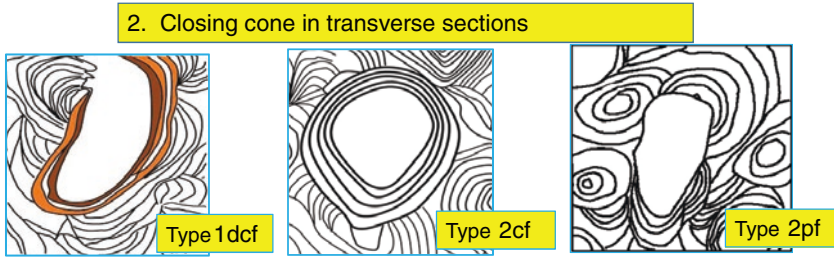
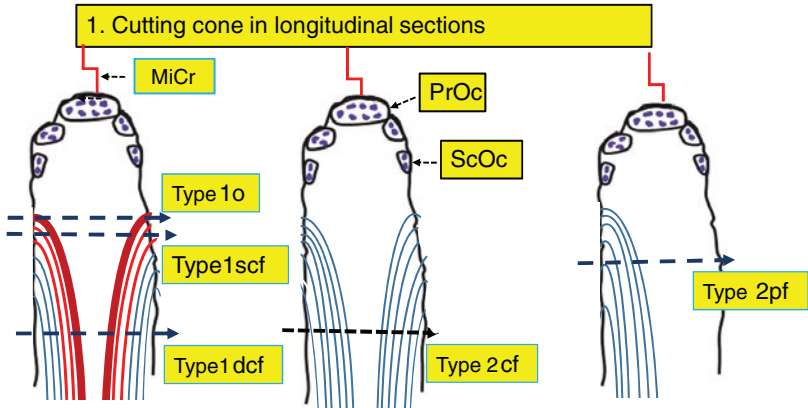
By ^cPolarized light

dLS: double label; OS: osteoid surface; ES: eroded surface, sLS: single label; IS: inert surface



Norimatsu: J Jpn Orthop Ass: 1971;45:415-430

Fig. 7 Secondary osteon with a cutting and closing cone (Reproduced with permission from Dr. Norimatsu and JOA). The secondary osteon in a rib of a metabolically normal dog. Undemineralized bone section, stained by Villanueva Tetrachrome stain, with double labeling. **1** shows a cutting cone of a secondary osteon advancing upward in the longitudinal section, under the bright light. “R” shows the resorptive phase, “R-R” is the resorptive-reversal phase in the cutting cone, and “F” is the formative phase of the closing cone of the remodeling cycle. The Haversian canal is observed in the middle of the closing cone and osteoid seam stained in green covers inner surface of the canal. **2** is observed under fluorescent light. Tetracycline appears as four yellow lines along the surface of the closing cone in the lower portion of the figure. The outer two lines are the first label and the inner lines are the second label. **3** is a transverse section of the closing cone, with the circumferentially forming bone surface. Osteoid is stained green. **4** shows the closing cone of the secondary osteon with partially forming surface and resorption on the opposite surface



Assessments of Endocortical Lamellar Bone

To assess the lamellar bone formed on the endocortical surface of the lateral cortex, the following parameters were measured, and indices calculated, expressed in terms defined by the ASBMR Nomenclature Committee [28]. In the L I, L II, and L III sections, endocortical lamellar bone area (EcLmB.Ar), maximum endocortical lamellar bone thickness (EcLmB.Th(max)), i.e., the maximum distance between the first layer of the lamellar bone and the surface of the osteoid seam (Fig. 11-2), and mean endocortical lamellar bone thickness (EcLmB.Th(mean)) were measured as EcLmB.Ar/EcLmB.S. Endocortical mineral apposition rate (EcMAR) was calculated as Interlabel width/Labeling period. Formation period (FP) of the endocortical lamellar bone of the L I section is calculated as EcLmB.Th/EcMAR.

3.3 Finite Element Analysis (FEA)

FEA was performed as reported in the previous study [27].

3.4 Statistical Analysis

A Chi-square test after a Ryan's multiple comparison test was performed for the number of the pores in the three sections to determine differences among 1d, 1s, 2, and 3 pores.

Non-parametric one-way ANOVA, Kruskal–Wallis test, and post hoc tests, Mann–Whitney U-tests with Bonferroni correction were used for comparison of

Fig. 8 Cutting cone in the longitudinal sections and closing cone in the transverse sections.

In osteonal remodeling there are five phases; activation, resorption, reversal/resorption, formation, and quiescence. In atypical femoral fracture cases it has been hypothesized that accumulation of microcracks activates resorption by targeted remodeling. A few osteoclasts make a cutting cone in which bone is resorbed (upward in this figure) by primary osteoclasts. These begin in existing canals or cavities and the canal/pore is widened by secondary osteoclasts along the walls of the cutting cone. **1** The upper schemas show cutting cones in longitudinal section. PrOc: Primary Osteoclast, ScOc: Secondary Osteoclast, MiCr: Microcrack. **2** The lower schemas show the closing cones in transverse section. Type 1: The cutting cone is followed by a closing cone with osteoid seam and labels. The number of labels or an osteoid seam without label depends on the level of the section. Type 1d pore is labeled twice, and the 1s pore is labeled only once. Type 1o indicates lamellar bone formation in the closing cone in which mineralization of new bone has not yet started. Type 2: The cutting cone is followed by a closing cone with lamellar bone formation, and the direction of lamellae is parallel to the inner surface of the pore. Formation can occur circumferentially over the entire pore, or partially, with the rest of the surface showing non-parallel lamellae. When formation has stopped before labeling, in transverse section, lamellar bone is observed without label and osteoid seam. **3** Type 3: The cutting cone in the longitudinal section is followed by a resorption cavity and remains without forming bone in the closing cone. **4** In transverse section no lamellar bone parallel to the inner surface is observed. **5** The type 4 pore is formed by coalescence of many large pores. The inner surface is composed with destructed osteons, interstitial lamellae, containing bone debris and effusion stained with a bone stain

pore size among types 1d, 1s, 2, and 3. These were also used for the comparison of pore size per mm² of the lateral cortex among these pore types. $P < 0.05$ and $p < 0.01$ were considered statistically significant for all analyses. R version 3.6.2 (The R Foundation for Statistical Computing, Austria) was used for all statistical analyses.

4 Results

4.1 Patient Clinical Outcome

Two weeks after surgery, low-intensity pulsed ultrasonography (LIPUS) [29] and daily Teriparatide (20 µg/day) therapy [30–32] were started to promote bone healing. The patient was permitted partial weight bearing 2 weeks post-operatively, and full weight bearing after 6 weeks. Three months post-operatively the plate was removed to prevent plate inhibition of bone healing. Ten months post-operatively the osteotomy site showed delayed union, but the patient developed an acute subarachnoid hemorrhage and died a week after the attack.

4.2 Bone Histomorphometry [28]

4.2.1 Measurements of Pores of the Lateral Cortex

The number of the four types of pores is shown in Fig. 9. The number of type 1s pores is the lowest, followed by type 1d and type 2 pores. Type 3 pores are the most common. The numbers of these four types are different statistically from each other.

The size and number of the four types of pores are shown in the plot-dot figures (Fig. 10-1, 2) showing the median values. Type 2 pores were the smallest type 3 pores have the highest median value. The porosity (TtPo.Ar/B.Ar) of the three sections (L I, L II, and L III/3) is 31.4%.

4.2.2 Enchondral Bone Formation

A zone of lamellar bone (EcLm.B) was observed on the endocortical surface of L I (Fig. 11). The maximum thickness of the zone was 848.26 µm and its mineral apposition rate was 0.85 µm/day. The formation period of the zone was about 1000 days. There is interruption of the lamellae at the middle of the endocortical surface, indicated with a red oval line. On the periosteal surface of L I, lamellar bone is not observed microscopically except for a remnant (Fig. 11-3), although an increase of periosteal thickness of the lateral cortex is recognized on the X-ray (Fig. 3-4). This was probably removed at surgery to make the femoral surface flat for plate fixation. Figure 11-4 shows a border between the original lateral cortex and the newly formed endocortical bone. In the figure there are five protuberances (indicated with yellow triangles) of lamellar bone into partially resorbed osteons in the lateral cortex, as if there were Howship's lacunae prior to formation of lamellar bone.

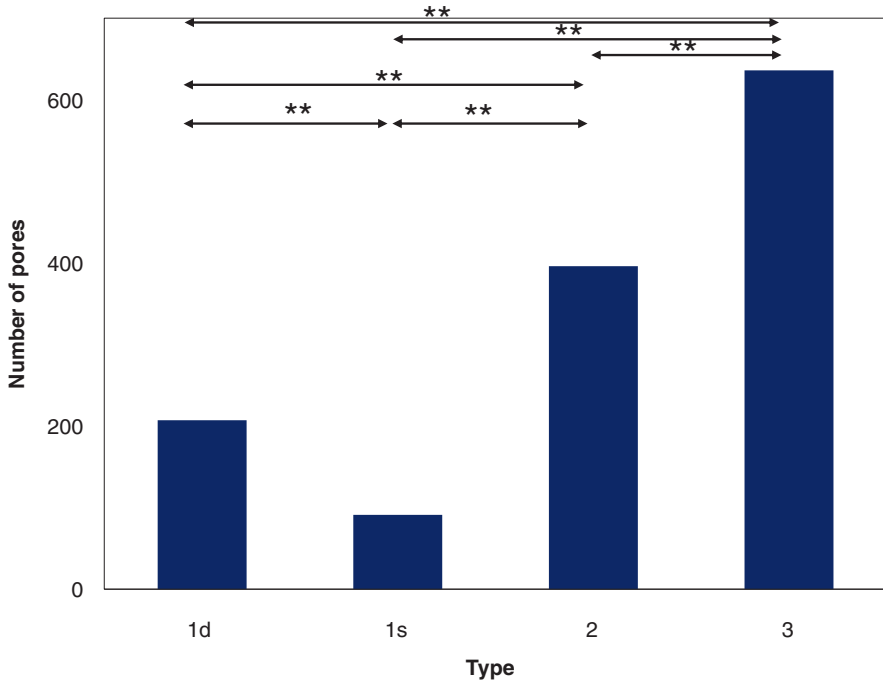


Fig. 9 Number of the Four Types of Pores. The number of the four types of pores is shown for all three sections. The number of each pore type is statistically different from the others

In about a half of the newly formed endosteal bone there are a few irregular lamellae, probably suggesting interlamellar breakage. They are not like scalloped cement lines or growth arrest lines. About one third of the lamellar bone seems to have been formed continuously on the wider area of the endosteal surface (Fig. 11-2, 04).

4.3 Comparison of Histomorphometric and FEA Findings

4.3.1 FEA Findings [27]

FEA color charts (Fig. 12) showed a marked tensile stress concentration on the lateral surface throughout the length of the femoral shaft. The mean values of MPS were 0.16 MPa on the medial cortex of the femoral shaft and 3.36 MPa on the lateral cortex. Maximum values of the MPS were 3.52 MPa on the medial cortex and 12.52 MPa on the lateral cortex. Therefore, comparing between medial cortex and lateral cortex, significantly large tensile stress was applied to the lateral cortex.

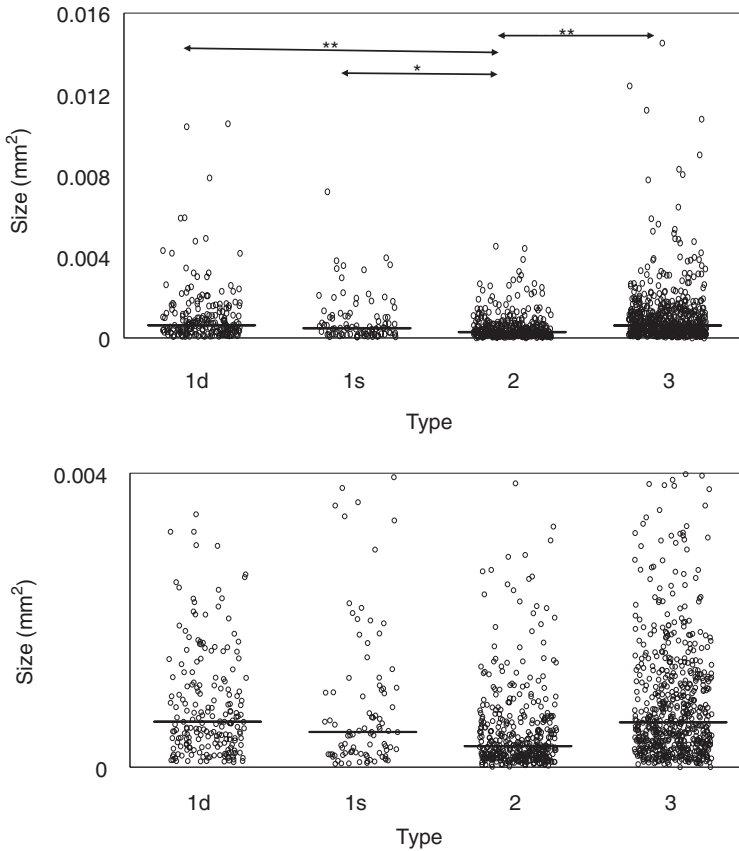


Fig. 10 Size and Number of the Four Types of Pores. The size and number of the four types of pores are shown in these plot-dot figures (1 in the high scale and 2 in the low scale) with the median values. Non-parametric one-way ANOVA, Kruskal–Wallis test, and post hoc tests, Mann–Whitney U-tests with Bonferroni correction were used for comparison of pore size and number. * $p < 0.05$ and ** $p < 0.01$ were considered statistically significant

4.3.2 Comparison among Histomorphometric Data, FEA and CT Findings [27]

Histomorphometric, FEA, and CT Findings

A bright light image of the L II section, FEA image, and CT image of the midshaft of the femur are compared in Fig. 13. The L II section (transverse direction) is just adjacent to the radiolucent line on X-ray in the area that has periosteal and endocortical hypertrophy. No periosteal bone formation is observed histologically. In

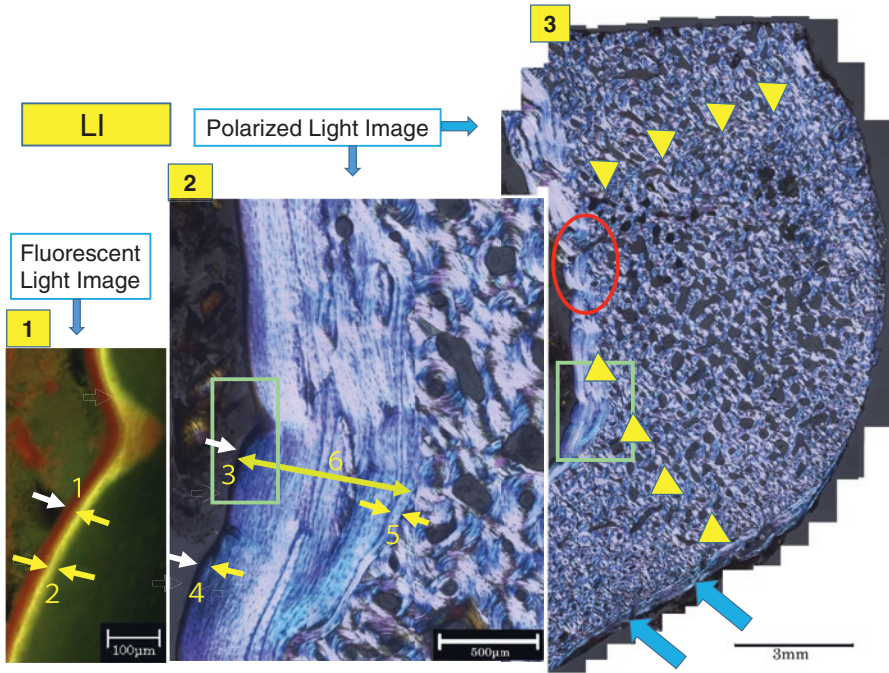


Fig. 11 Multiporous Area of the Lateral Cortex and Lamellar Bone Formation on the Osteonal Surface. L I section is about 1 mm apart from the radiolucent line. **1** A fluorescent light image shows the endocortical surface of the lateral cortex bordered by the marrow cavity. Most superficially is the osteoid seam (deep red, numeral 1), pinched by two short white and yellow arrows. The next layer is a single yellow label (numeral 2), pinched by a pair of yellow arrows. Although this label looks like single label, it is microscopically observed as double because of the thickness of the ground section (30 μ m). **2** An enlarged image of the endocortical surface of the lateral cortex under polarized light shows endocortical lamellar bone to the left and compact bone with enlarged pores to the right. The numeral 3 indicates the osteoid surface by the white arrow. The numeral 4 indicates the osteoid seam, shown by a pair of white and yellow arrows. The numeral 5 indicates the first lamellar layer, bordered with the compact bone. The numeral 6, a double headed yellow bar, indicates the maximum endocortical lamellar bone thickness (EcLMB.Th). The first layer numbered 5 was formed about 2.7 years prior to the osteotomy and the osteoid seam numbered 4 is being formed at the time of the corrective osteotomy. **3** This is a collective image of about 200 visual fields at $\times 100$ magnification under polarized light. There are many large pores in the triangular area of the lateral cortex, surrounding the point of interrupted lamellar bone, indicated by a red oval on the endocortical surface. On the periosteal surface at the lower part of the cortex, the remnants of lamellar bone are indicated by the blue arrows. **4** This figure shows a border between the original lateral cortex and the newly formed endocortical bone. In the figure there are five protuberances (yellow triangles) of lamellar bone into partially resorbed osteons, as if there were Howship's lacunae prior to formation of lamellar bone. The numeral 1 in the lamellar bone is a round resorption cavity. The numeral 2 shows interlamellar breakage and 3 shows lamellar interruption

4. A border between original cortex and newly formed endocortical bone of the lateral cortex

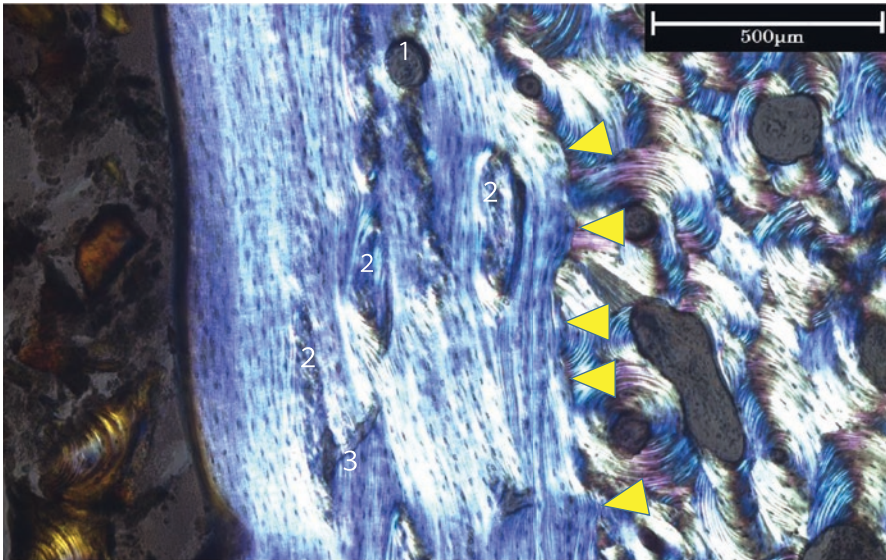


Fig. 16.11 (continued)

the upper one quarter of the section is a type 4 pore, which contains fragmented lamellar bone and debris. The middle half of the cortex contains many enlarged pores of types 1, 2, and 3. The lower quarter of the lateral cortex contains normal sized pores. Endocortical Lamellar Bone (EcLmB) is indicated by four pairs of blue arrows. The red part of FEA image of the lateral cortex takes up less than half of the entire image, shown in Fig. 13-2. But when the image is limited in the same area as the bone section, about three quarters of the area is under tensile load. A CT image of the midshaft of the femur also shows the thickness of the lateral cortex. The anterior part of the cortex is not included in the section as it was left on the edge of the shaft to create stability for fixation from the osteotomy and intramedullary nailing.

Comparison of Size and Numbers of Pores Between Tensile and Compressive Force

The section of the lateral femoral cortex was divided into four areas. The anterior three quarter areas correspond to the tensile area (red in FEA) and the posterior quarter area corresponds to the compressive area (light green). The size and number of each pore was divided by areas of the section and expressed per mm^2 . Comparison of type and numbers of each pore per mm^2 between the tensile area (Tn.Ar) and the compressive area (Cm.Ar) was made. Figure 14 shows that the size and numbers of each pore are larger in the tensile area than in the compressive area.

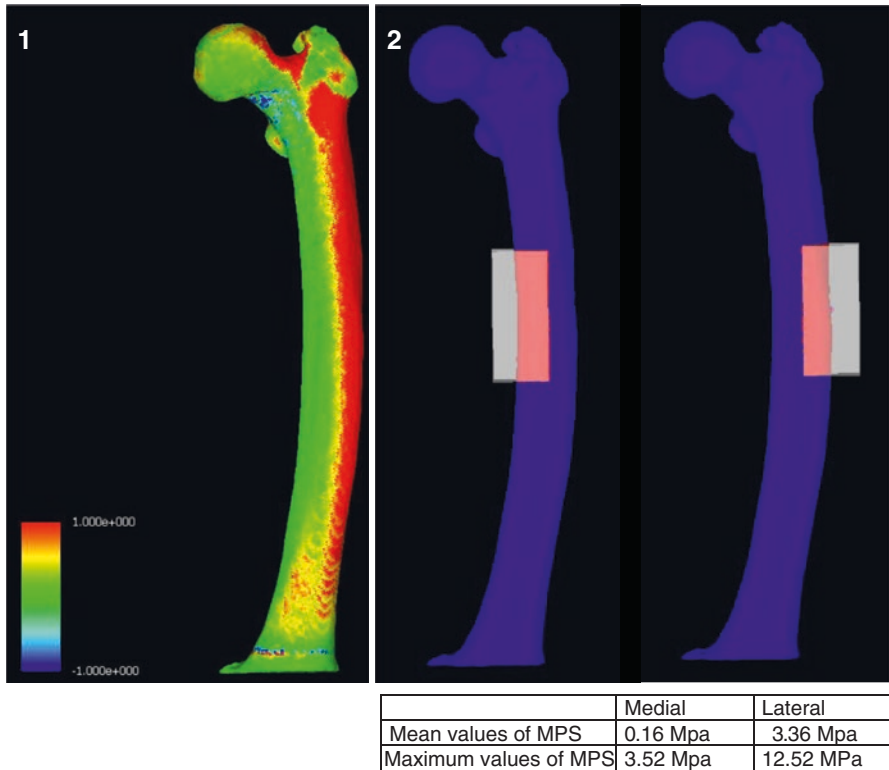


Fig. 12 Results of the FEA. (a) FEA showed a marked tensile stress concentration (red color) on the lateral surface of the femoral shaft under loading patient’s weight. (b) Maximum and mean values of maximum principal stress(MPS) were analyzed by data extraction from a 70 mm section in the middle of the femoral diaphysis. MPS on the lateral cortex was higher than that on the medial cortex

5 Discussion

We will discuss histomorphometric findings showing the presence of many enlarged pores focally in the lateral cortex, together with possible disturbance of bone formation in a remodeling cycle. In recent years our understanding of the initiation and structure of a secondary osteon and the sequence of events in cortical remodeling [33–38] has been deepened.

Microcracks and Targeted Remodeling

At the beginning of osteonal remodeling in cortical bone, microcracks produced by mechanical loading are targeted by osteoclasts for resorption. These osteoclasts in the tip of the cutting cone, called primary osteoclasts, are responsible for the longitudinal advancement at a rate of about 40 to 50 $\mu\text{m}/\text{day}$ [39–41]. Mashiba et al. demonstrated that suppression of his process allows microdamage to accumulate, leading to reduced bone toughness in the rib cortex of dogs [42].

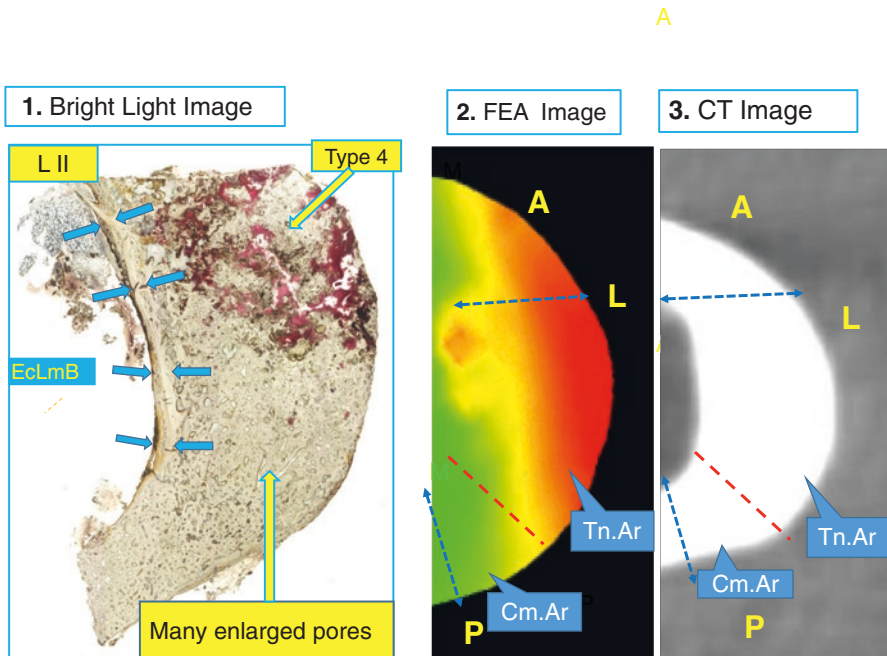


Fig. 13 Comparison of three images of the lateral cortex. **1** A bright light image of section L II (transverse direction) just next to the radiolucent line on X-ray with periosteal and endocortical hypertrophy. No periosteal bone formation is observed histologically. In the upper one quarter of the section is a type 4 pore, which contains fragmented lamellar bone and debris. The middle half of the cortex contains many enlarged pores of types 1, 2, and 3. The lower quarter of the lateral cortex contains normal sized pores. Endocortical Lamellar Bone (EcLmB) is indicated by four pairs of blue arrows. **2** The red part of FEA image takes up less than half of the image, and about three quarters of the area of bone section is under tensile force on the FEA image. The anterior part of the cortex is not included in the section as it was left on the edge of the shaft to create stability for fixation from the osteotomy and intramedullary nailing. **3** A CT image of the midshaft of the femur. A: anterior; P: posterior, and L: lateral

Presence of Reversal-Resorptive Phase

After longitudinal extension of the cutting cone in the initial resorption phase, Delaisse's group [43–47] proposed a reversal-resorptive (RvRs) phase in which reversal cells and osteoclasts appeared on the wall of the tunnel portion of the cutting cone. These secondary osteoclasts play a role in widening the cutting cone. Based on cutting cones obtained from femurs of 9 patients and fibulae of 10 patients, Lassen et al. [46] showed that bone matrix was subjected to several resorption episodes, separated by reversal periods during which increasing numbers of reversal/osteoprogenitor cells were recruited. The density of osteoprogenitors continuously grew along the “reversal/resorption” surface, reaching at least 39 cells/mm on initiation of bone formation. This value was independent of the length of the reversal/resorption surface. These observations strongly suggest that bone formation is initiated only above a threshold cell density, that the length of the reversal/resorption

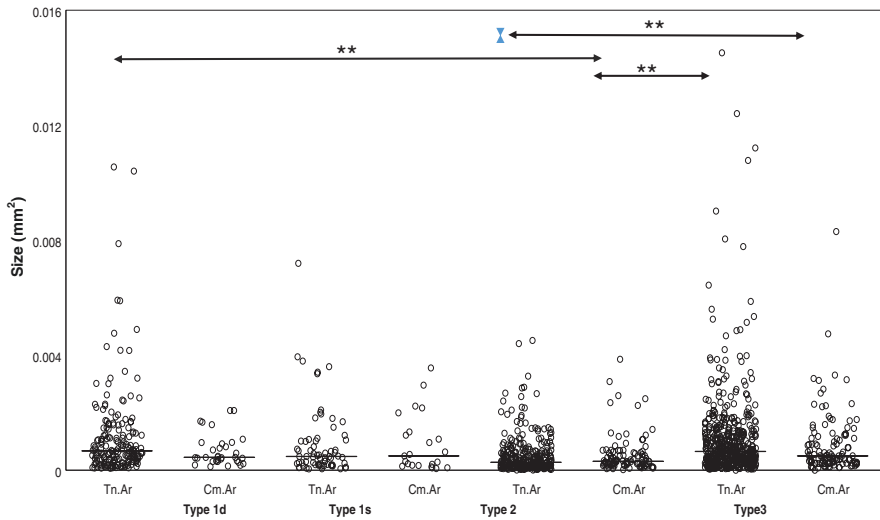


Fig. 14 Comparison of Size and Number of Four Types of Pores between Tensile and Compressive Area. Lateral femoral cortex was divided into four areas. The anterior three quarter areas correspond to the tensile area (red in FEA) and the posterior quarter area corresponds to the compressive area (light green). The size and number of each pore was divided by areas of the section and expressed per mm². Comparison of type and numbers of each pore per mm² between Tensile Area (Tn.Ar) and Compressive Area (Cm.Ar) was made. Non-parametric one-way ANOVA, Kruskal–Wallis test, and post hoc tests, Mann–Whitney U-tests with Bonferroni correction was used for the comparison of pore size per mm² of the lateral cortex among pore type 1d, 1s, 2, and 3. * $p < 0.05$ and ** $p < 0.01$ were considered statistically significant

period depends on how fast osteoprogenitor recruitment reaches this threshold, and thus that the slower the rate of osteoprogenitor recruitment, the more bone is degraded. Once a threshold of reversal/osteoprogenitor cell density is reached, bone formation is initiated, and resorption is switched off. They proposed a model in which the rate of reversal/osteoprogenitor cell recruitment slows the extent of resorption.

Widespread Variation of Reversal/Resorptive Phase

In this case the amount of cortical bone resorbed in osteonal remodeling in the lateral cortex through both initial and secondary resorption is not clear, but secondary osteoclasts may play a major role in increasing pore size. Lassen et al. [46] also reported widespread variation in the absolute length of the RvRs zone among measured BMUs, indicating great variations in the time lag for starting bone formation after the period of initial resorption (fivefold variation between the smallest and the largest RvRs length). The longer the RvRs surface, the larger the diameter of the cutting cone. Norimatsu [39] examined 298 cutting cones of long tubular bones of fore- and hindlimbs and ribs of mongrel dogs and reported a high correlation ($r = 0.48 \sim 0.90$, $p < 0.001 \sim 0.002$) between the linear rate of longitudinal bone resorption and osteon diameter [39, 41]. This relation reflects that the longer the exposure of the RvRs surface to osteoclasts, the more bone is removed. The

osteoblast density at the onset of bone formation is independent of the length of the RvRs of different cutting cones [46]. In this case there is also a large variation of pore size in the lateral cortex.

Successive Bone Formative Phase

Bisphosphonates strongly inhibit bone resorption, but also strongly decrease bone formation. The decreased formation is commonly thought to be due to the mechanism maintaining the resorption/formation balance during a remodeling cycle. Jensen et al. [47] have morphometrically reported an additional mechanism where a bisphosphonate impairs in slowing down the recruitment of osteoprogenitors on the eroded surface, thereby putting at risk initiation of bone formation after resorption, and strongly decreases the activation frequency of bone formation and decreases more the formative than the eroded surfaces. It seems that bisphosphonates hamper the osteoprogenitor recruitment required to initiate bone formation.

Although pore size is increased, in this case, the pore can still form lamellar bone with double or single label (type 1d and 1s pores), observed in the periphery of the lateral cortex of the L I section (Fig. 5). Small pores show the largest number of type 1 pores, although type 1 pores can also be larger (Fig. 10-1, 2). Large 1d and 1s type pores are six- to sevenfold larger than the median size, but still maintain the capability for bone formation, suggesting that “once a threshold reversal/osteoprogenitor cell density is reached, bone formation is initiated and resorption is switched off” (Lassen et al. [46]). The pores with lamellar bone covering the inner surface of the pore without label may suggest cessation of bone formation prior to labeling (type 2 pore). Type 2 pores not only have parallel lamellae with bone formation on the entire inner surface, but some pores show formation only on a part of the inner surface; the rest of the inner surface could be inert (Fig. 4). This probably means that the reversal/osteoprogenitor cell density locally is different within the pore. Pores without lamellar bone formation on their inner surface were named type 3 pores. When secondary osteoclasts have a long lifespan or are successively recruited, the widening may continue over a prolonged period. When secondary osteoclasts are not recruited, widening stops, and no successive bone formation occurs (type 3, Fig. 4).

When bone formation is switched on, the osteon closes radially and forms the Haversian canal. The MAR of type 1d pores is normal, but bone formation does not persist to create a normal sized Haversian canal. Based on the cross-sectional area of rib osteons from 20 to 70 years of age (Landeros et al. [48]), and femoral osteon size of an 80-year-old female (Yamamoto et al. [49]), the cross-sectional area of the Haversian canal is about 10% of the cross-sectional area of the secondary osteon. Pore size is much larger than normal canal size, probably due to incomplete coupling and poor osteoprogenitor cell density.

In this case Teriparatide was used to treat AFF, which has been reported to reduce bone microdamage accumulation in patients with osteoporosis [50]. Teriparatide increases the numbers of early cells of the osteoblast lineage, hastens their differentiation into osteoblasts, and suppresses their differentiation into adipocytes in vivo [51].

Development of Pores and Their Coalescence

Bisphosphonates used to treat osteoporosis decrease osteoclast function, resulting in accumulation of microcracks [42], which might cause weakness of the femoral shaft resulting in atypical femoral fracture [6]. In this case targeted remodeling of microcracks developed into large pores with widespread variation. Although lamellar bone was still forming at the time of biopsy in type 1 pores, insufficient bone was formed in type 2 pores and no bone formation occurred in type 3 pores. This may suggest incomplete or no coupling had occurred just after the reversal/resorption phase. A radiolucent fracture line between the L II and L III sections revealed a region where coalescence of pores had occurred, resulting in large type 4 pores containing fragments of destroyed lamellar structure and debris.

Periosteal and endocortical lamellar bone formation

In osteonal remodeling lamellar bone is formed. Intracortical bone loss near and at the fracture line of the lateral cortex, where type 4 pores accumulated in a narrow portion of the shaft may have weakened the bone, resulting in compensatory periosteal and endocortical lamellar bone formation that began 3 years prior to osteotomy, although this may be still underestimated. On both periosteal and endocortical surfaces thickening of bone was radiologically observed in the transverse radiolucent linear zone. A border between the original lateral cortex and the newly formed endosteal lamellar bone may be a type of “cement line” [52, 53]. It seems, in this case, endosteal lamellar bone formation is modeling-based formation, starting with resorption of the lateral cortex, but not remodeling-based formation.

There are only a few reports on bone histomorphometric findings at the fracture site in AFF. Jamal et al. [17] have confirmed bone formation after tetracycline double labeling in a specimen obtained just below the point of fracture. Schilcher et al. [19] reported histology of eight cases of AFF, which revealed channels along the fracture line in longitudinal sections. Oh et al. [24] also assessed local bio-activity and demonstrated many enlarged resorptive cavities.

These findings are consistent with what we have found in the lateral cortex of the femur. In our previous study [27] we also demonstrated the tensile stress of the femoral shaft and showed that the maximum principal stress differs significantly between the medial and lateral cortices. Furthermore, when the bone cross-section was compared to the CT axial slice and the axial image from the FEM, type 4 pores had accumulated at the tensile stress concentration site on the lateral femoral cortex (Fig. 13). The patient's age and the low value of 25(OH)vitamin D (Table 1) may have played some role in the severe bowing [54].

With histological findings, FEA and CT images, the following hypothesis of development of AFF may be considered in this case (Fig. 15). Tensile force in the bowed femur prolongs the activity of secondary osteoclasts, resulting in enlarged pores. Insufficient bone formation does not refill the resorption cavity probably due to incomplete or absent coupling in remodeling. Coalescence of many enlarged pores allows a fracture line to develop, and leads to subsequent fracture.

Suppression of bone remodeling by bisphosphonates allows accumulation of microdamage [42]. With targeted remodeling primary osteoclasts initiate resorption

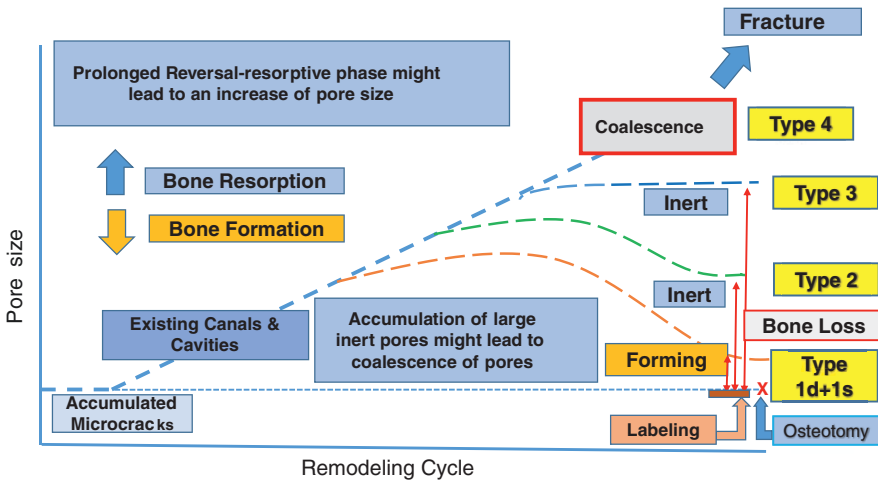


Fig. 15 Prolongation of reversal-resorptive phase and accumulation of large inert pores might lead to coalescence of pores, and subsequent fracture. With histological findings, FEA and CT images, the following hypothesis of development of AFF may be considered in this case. Accumulated microcracks might have initiated bone resorption as cutting cones in targeted remodeling, which have grown into existing canals and cavities. In the focal biomechanical environment of the lateral cortex remodeling might lead to prolongation of the reversal-resorptive phase, resulting in increased pore size. Subsequently, BMUs might start bone formation, and continue to form lamellar bone until the period of labeling (type 1 pore). Some BMUs might have switched from bone resorption to bone formation but stopped in the formative phase before labeling. Thereafter, the inner surface of the pore would be inert, with neither resorption nor formation (type 2 pore). Other BMUs might have started to resorb bone, and stopped resorption, but did not switch to bone formation. Then the inner surface of the pore would be inert (type 3 pore). All these BMUs had increased bone resorption, resulting in increased pore size, but did not refill completely the amount of bone lost. Consequently, most of BMUs in the lateral cortex have changed to many large inert pores. These pores might become larger by coalescence, and lead to subsequent fracture

of the microdamage. In the focal biomechanical environment of the lateral cortex (Fig. 12) the remodeling might lead to prolongation of the reversal-resorptive phase, when secondary osteoclasts at the side wall of the cone work to widen the diameter of the cone resulting in increased pore size (Fig. 5). Then BMUs might start bone formation and continue to form lamellar bone until the period of labeling (type 1 pore, Fig. 4). Type 1 pores can still form lamellar bone so the amount of bone loss may be small. Some BMUs might have switched from bone resorption to bone formation but stopped in the formative phase before labeling. Thereafter, the inner surface of the pore would be inert (type 2 pore, Fig. 6-1,-2). As type 2 pores had stopped bone formation, there may be less bone formed than resorbed. Other BMUs might have started to resorb bone but did not switch to bone formation. Then the inner surface of the pore would be inert (type 3 pore, Fig. 6-3). After the reversal-resorptive phase the type 3 pore became inert and so loss of bone on these surfaces might be the largest among the three types of pores (Figs. 9, 10-1, 2). All these BMUs had increased bone resorption but did not refill sufficiently with new bone to

replace all the bone that was lost. Consequently, most BMUs in the lateral cortex have changed to large inert pores, with neither active resorption nor formation. These pores might become larger by coalescence (type 4, Figs. 6-4, 5, 8-5, 11-3, 13-1). Size and numbers of pores are larger in the tensile area than in the compressive area (Fig. 14). Although bowing and hypovitaminosis D may play additional roles, enlarged pores can be observed in the cortical bone for about 1 cm in length (Fig. 3-3). Concentration of coalescence occurs in about 1 mm thickness of the lateral cortex and leads to subsequent fracture. Although the patient had been administered a bisphosphonate 5 years prior to the fracture, she had started to have enlargement of pore size in the lateral cortex more than 3 years (Fig. 11) prior to the osteotomy.

This study had some limitations. First, this was a study of only one case. We sometimes encounter AFF and perform surgery, but it is common to treat AFFs with intramedullary nailing alone, and it is not easy to collect nearly circumferential cortical bone from the fracture site. Second, the clinical course of this fracture is unknown due to the patient death.

6 Summary

The presence of large pores in regions of developing AFFs may mean prolonged activity of secondary osteoclasts, together with loss of complete or incomplete coupling with bone formation. With the gradual accumulation of large pores and their coalescence, in combination with high tensile stresses on the lateral femoral cortex, an AFF eventually developed.

Ethics This study was approved by the institutional review board of the second author's institution. We obtained consent from the patient, complying with the principles laid down in the Declaration of Helsinki. Our report of the patient is completely anonymous, protecting the privacy and dignity of the patient.

References

1. Odvina CV, Zerwekh JE, Rao DS, et al. Severely suppressed bone turnover: a potential complication of alendronate therapy. *J Clin Endocrinol Metab.* 2005;90:1294–301.
2. Starr J, Tay YKD, Shane E. Current understanding of epidemiology, pathophysiology, and management of atypical femur fractures. *Rev Curr Osteoporos Rep.* 2018;16:519–29.
3. Neviaser AS, Lane JM, Lenart BA, et al. Low-energy femoral shaft fractures associated with alendronate use. *J Orthop Trauma.* 2008;22:346–50.
4. Yang SP, Kim TW, Boland PJ, et al. Retrospective review of atypical femoral fracture in metastatic bone disease patients receiving Denosumab therapy. *Oncologist.* 2017;22(4):438–44.
5. Shane E, Burr D, Ebeling PR, et al. Atypical subtrochanteric and diaphyseal femoral fractures: report of a task force of the American Society for Bone and Mineral Research. *J Bone Miner Res.* 2010;25:2267–94.

6. Shane E, Burr D, Abrahamsen B, et al. Atypical subtrochanteric and diaphyseal femoral fractures: second report of a task force of the American Society for Bone and Mineral Research. *J Bone Miner Res.* 2014;29:1–24.
7. Larsen MS, Schmal H. The enigma of atypical femoral fracture: a summary of current knowledge. *EFORT OPEN Rev.* 2018;3(9):494–500.
8. Kwek EB, Goh SK, Koh JS, et al. An emerging pattern of subtrochanteric stress fractures: a long-term complication of alendronate therapy? *Injury.* 2008;39:224–31.
9. Lenart BA, Neviasser AS, Lyman S, et al. Association of low energy femoral fractures with prolonged bisphosphonate use: a case control study. *Osteoporos Int.* 2009;20:1353–62.
10. Mohan PC, Howe TS, Koh JS, et al. Radiographic features of multifocal endosteal thickening of the femur in patients on long term bisphosphonate therapy. *Eur Radiol.* 2013;23:222–7.
11. Sato H, Kondo N, Wada, et al. The cumulative incidence of and risk factor for latent beaking in patients with autoimmune diseases taking long-term glucocorticoids and bisphosphonates. *Osteoporos Int.* 2016;27(3):1217–25. <https://doi.org/10.1007/s00198-015-382-9>.
12. Hagino H, Endo N, Yamamoto T, et al. Treatment status and radiographic features of patients with atypical femoral fracture. *J Orthop Sci.* 2018;23(2):316–20.
13. Kumar G, Dhamangaonkar AC. Bisphosphonate associate femoral stress fracture distal to an orthopaedic implant: they are predictable ! Case reports. *J Cli Orthop Trauma.* 2019(Suppl. 1):S112–4.
14. Tan J, Sano H, Poole K. Antiresorptive-associated spontaneous fractures of both tibiae, followed by an atypical femur fracture during the sequential treatment with alendronate, denosumab then teriparatide. *BMJ Case Rep.* 2019;12(7):e229366. <https://doi.org/10.1136/bcr-2019-229366>
15. Somford MP, Draaijer FW, Thomassen BJ, et al. Bilateral fractures of the femur diaphysis in a patient with rheumatoid arthritis on long-term treatment with alendronate: clues to the mechanism of increased bone fragility. *J Bone Miner Res.* 2009;24(10):1736–40.
16. Aspenberg P, Schilcher J, Fahlgren A. Histology of an undisplaced femoral fatigue fracture in association with bisphosphonate treatment. *Acta Orthop.* 2010;81(4):460–2.
17. Jamal SA, Dion N, Ste-Marie LG. Atypical femoral fractures and bone turnover. *N Engl J Med.* 2011;365:1261–2.
18. Kajino Y, Kabata T, Watanabe K, et al. Histological finding of atypical subtrochanteric fracture after long-term alendronate therapy. *J Orthop Sci.* 2011;17(3):313–8.
19. Schilcher J, Sandberg O, Isaksson H, et al. Histology of 8 atypical femoral fractures remodeling but no healing. *Acta Orthop.* 2014;85(3):280–6.
20. Schilcher J: Personal communication.
21. Kondo N, Fukuhara T, Watanabe Y, et al. Bone formation parameters of the biopsied ilium differ between subtrochanteric and diaphyseal atypical femoral fractures in bisphosphonate-treated patients. *Tohoku J Exp Med.* 2017;243(4):247–54.
22. Oh Y, Wakabayashi Y, Kurosa Y, et al. Potential pathogenic mechanism for stress fractures of the bowed femoral shaft in the elderly: mechanical analysis by the CT based finite element method. *Injury.* 2014;45:1764–71.
23. Oh Y, Fujita K, Wakabayashi Y, et al. Location of atypical femoral fracture can be determined by tensile stress distribution influenced by femoral bowing and neck shaft angle: a CT-based nonlinear finite element analysis model for the assessment of femoral shaft loading stress. *Injury.* 2017;48:2736–43.
24. Oh Y, Yamamoto K, Hashimoto J, et al. Biological activity is not suppressed in mid-shaft stress fracture of the bowed femoral shaft unlike in “typical” atypical subtrochanteric femoral fracture: a proposed theory of atypical femoral fracture subtypes. *Bone.* 2020;137:115453. <https://doi.org/10.1016/j.bone.2020.115453>.
25. Villanueva AR, Lundin KD. A versatile new mineralized bone stain for simultaneous assessment of tetracycline and osteoid seams. *Stain Technol.* 1989;64:129–38.
26. Villanueva AR. Preparation and staining of mineralized sections of bone. In: Takahashi HE, editor. *Handbook of bone morphometry.* 2nd ed. Niigata: Nishimura Publisher; 1997. p. 27–40.

27. Hirano F, Okuma KF, Zenke Y, et al. Disturbance of osteonal bone remodeling and high tensile stresses on the lateral cortex in atypical femoral fracture after long-term treatment with risendronate and alfacalcidol for osteoporosis. *Bone Rep.* 2021;101091 <https://doi.org/10.1016/j.bonr.2021.101091>.
28. Dempster DW, Compston JE, Drezner MK, et al. Standardized nomenclature, symbols, and units for bone Histomorphometry: a 2012 update of the report of the ASBMR Histomorphometry nomenclature committee. *J Bone Miner Res.* 2013;28(1):1–16. <https://doi.org/10.1002/jbmr.1805>.
29. Lou S, Lv H, Li Z, et al. The effects of low-intensity pulsed ultrasound on fresh fracture: a meta-analysis. *Medicine (Baltimore).* 2017;96(39):e8181.
30. Greenspan SL, Vujević K, Britton C, et al. Teriparatide for treatment of patients with bisphosphonate-associated atypical fracture of the femur. Randomized controlled trial. *Osteoporos Int.* 2018;29(2):501–6.
31. Kendle DL, Marin F, Zerbini CAF, et al. Effects of teriparatide and risendronate on new fractures in post-menopausal women with severe osteoporosis (VERO): a multicentre, double-blind, double-dummy, randomised controlled trial. *Lancet.* 2018;391(10117):230–40. [https://doi.org/10.1016/S0140-6736\(17\)32137-2](https://doi.org/10.1016/S0140-6736(17)32137-2)
32. Tachie H, Miyakoshi N, Iba K, et al. The effects of teriparatide on acceleration of bone healing following atypical femoral fracture: comparison between daily and weekly administration. *Osteoporos Int.* 2018;29(12):2659–65.
33. Frost HM. Presence of microscopic cracks in vivo in bone. *Henry Ford Hosp Med Bull.* 1960;8(1):25–35.
34. Mori S, Burr DB. Increased intracortical remodeling following fatigue damage. *Bone.* 1993;14:103–9.
35. Burr DB, Forwood MR, Fyhrie DP, et al. Bone microdamage and skeletal fragility in osteoporotic and stress fractures. *J Bone Miner Res.* 1997;12(1):6–15.
36. Parfitt AM. Targeted and nontargeted bone remodeling: relationship to basic multicellular unit origination and progression. *Bone.* 2002;30(1):5–7.
37. Diab T, Vashishth D. Morphology, localization and accumulation of in vivo microdamage in human cortical bone. *Bone.* 2007;40(3):612–8.
38. Harrison KD, Cooper DM. Modalities for visualization of cortical bone remodeling: the past, present and future. *Front Endocrinol.* 2015;6:122. <https://doi.org/10.3389/fendo.2015.00122>
39. Norimatsu H. A linear rate of longitudinal resorption, and number and surface area of actively forming secondary osteons in the cortical bone. *J Jap Orthop Ass.* 1971;45:415.
40. Jaworski ZF, Lok E. The rate of osteoclastic bone erosion in Haversian remodeling sites of adult dog's rib. *Calcif Tiss Res.* 1972;10:103–12.
41. Takahashi H, Norimatsu H. The longitudinal and transverse rate of resorption of the Haversian systems in canine bone. In: *Proceedings of the first workshop on bone morphometry.* Jaworski ZFG (ed). Univ Ottawa Press, 1976; 143–147.
42. Mashiba T, Hirano T, Turner CH, et al. Suppressed bone turnover by bisphosphonates increases microdamage accumulation and reduces some biomechanical properties in dog rib. *J Bone Miner Res.* 2000;15(4):613–20. <https://doi.org/10.1359/jbmr.2000.15.4.613>.
43. Delaisse JM. The reversal phase of the bone remodeling cycle: cellular prerequisites for coupling resorption and formation. *Bonekey Rep.* 2014 (review).
44. Andersen TL, Abdelgawad ME, Kristensen HB, et al. Understanding coupling between bone resorption and formation: are reversal cells the missing link? *Am J Pathol.* 2013;183(1):235–46. <https://doi.org/10.1016/j.ajpath.2013.03.006>.
45. Abdelgawad HE, Delaisse JM, Hinge M, et al. Early reversal cells in adult human bone remodeling: osteoblastic nature, catabolic functions and interactions with osteoclasts. *Histochem Cell Biol.* 2016;145(6):603–15. <https://doi.org/10.1007/s00418-016-1414-y>
46. Lassen NE, Andersen TL, Ploen GG, et al. Coupling of bone resorption and formation in real time: new knowledge gained from human Haversian BMUs. *J Bone Miner Res.* 2017:1–11. <https://doi.org/10.1002/jbmr.3091>.

47. Jensen PR, Andersen TL, Chavassieux P, et al. Bisphosphonates impair the onset of bone formation at remodeling sites. *Bone*. 2021;145:115850. <https://doi.org/10.1016/j.bone.2021.115850>.
48. Landeros O, Frost HM. The cross section size of the osteon. *Henry Ford Hosp Med Bull*. 1964;12:517–25.
49. Yamamoto K, Okuno M, Nakamura T, et al. Deterioration of microstructure in compact bone associated with femoral neck fracture—morphometric analysis of contact microradiographs (CMRs). *J Jpn Osteoporos Soc*. 2018;4:323–32 (Japanese).
50. Dobnig H, Stepan JJ, Burr DB, et al. Teriparatide reduces bone microdamage accumulation in postmenopausal women previously treated with alendronate. *J Bone Miner Res*. 2009;24(12):1998–2006.
51. Balani DH, Ono N, Kronenberg HM. Parathyroid hormone regulates fates of murine pre-osteoblast precursors in vivo. *J Clin Invest*. 2017;127(9):3327–38. <https://doi.org/10.1172/JCI91699>.
52. Skedros JG, Holmes JL, Vajda EG, et al. Cement lines of secondary osteons in human bone are not mineral-deficient: new data in a historical perspective. *Anat Rec A Discov Mol Cell Evol Biol*. 2005;286(1):781–803. <https://doi.org/10.1002/ar.a.20214>
53. Okada H, Tamamura R, Kanno T, et al. Ultrastructure of cement lines. *J Hard Tissue Biol*. 2013;22(4):445–50. <https://doi.org/10.2485/jhtb.22.445>
54. Tsuchie H, Miyakoshi N, Kasukawa Y, et al. Factors related to curved femur in elderly Japanese women. *Ups J Med Sci*. 2016;121(3):170–3. <https://doi.org/10.1080/03009734.2016.1185200>.